UNIVERSITÀ DEGLI STUDI DI PADOVA
Facoltà di Scienze MM.FF.NN.
Facoltà di Ingegneria

ISTITUTO NAZIONALE DI FISICA NUCLEARE
Laboratori Nazionali di Legnaro

in collaboration with Confindustria Veneto

MASTER THESIS
in
"Surface Treatments for Industrial Applications"

Titanium nitride coating by reactive DC magnetron sputtering as a multipactor suppressor on coupler RF ceramic windows

Supervisor: Pr. V. PALMIERI
Dr. A. VARIOLA

Student: Walid KAABI
Matr. N°: 88 49 72

Academic Year 2007-08

Contents

Introduction

Chapter I: Fundamentals and study's Framework

I- Power coupler for supraconductive cavities

I-1- Role of power coupler for superconductive cavities

I-1-1- Electromagnetic role

I-1-2- Vacuum barrier

I-1-3- Thermal interface

I-2- Power coupler design: example of TTF-III model

I-2-1- Cold part

I-2-2- Warm part

I-2-3- Wave guide transition

I-3- Behaviour of coupler in RF power exposure

I-3-1- Excessive electric field

I-3-2- Degassing

I-3-3- Multipacting

II- Coupler ceramic windows

II-1- Secondary electron emission yield

II-2- Multipactor Phenomenon

II-2-1- Description of multipactor discharge

II-2-2- Conditions for multipactor establishment

II-2-3- Mechanisms and order of multipactor

II-2-4- Multipactor damages on Alumina windows

III- Multipactor suppressor thin film

IV- DC Reactive magnetron sputtering

IV-1- Basics of sputtering deposition

IV-2- Basics of reactive sputtering

IV-2-1- Interest and advantages

IV-2-2- Target poisoning and hysteresis effect

Chapter II: Titanium nitride sputtering system

I- Particular requirements for sputtering system

I-1- General requirements

I-2- Deposit quality

I-3- Pumps, vacuum chamber and vacuum control system

I-4- Process and controls

II- Sputtering system description

II-1- Pumping and vacuum control system

II-2- Vacuum chamber

II-3- Targets and magnet packs

II-4- Sample holder

II-5- Front panel: controls and racks

Chapter III: Results and discussions

I- Practical guidance’s

II- Parameters optimization for a stoichiometric deposit

III- Deposition rate variation with process pressure

IV- Thickness control of stoichiometric deposit

V- Influence of substrate-target distance on sputtered films

V-1- Influence on deposit stoichiometry

V-1 Influence on deposit thickness

Conclusions

Introduction

Introduction

LAL-Orsay is developing an important effort on R&D and technology studies on RF power couplers for superconductive cavities. These are complex and high technology devices due to their basic functions: RF power matching between source and cavity, vacuum and temperature separation from the environment to the cavity. One of the most critical components of high power couplers is the RF ceramic window that allows the power flux to be injected in the coaxial line. The presence of a dielectric window on an RF power line has in fact a strong influence on the multipactor phenomena, a resonant electron discharge that is strongly limiting for the RF components performances. The most important method to reduce the multipactor is to decrease the secondary emission yield of the ceramic window. Due to its low secondary electron emission coefficient, TiN thin film is used as a multipactor suppressor coating on ceramic coupler windows. In addition, TiN permits to drain away electric charges on the surfaces to avoid material break down.

In this framework, a sputtering machine was developed allowing thin layer titanium nitride coating on ceramic. The coupler operating conditions, the physical properties of TiN layer and alumina substrate in addition to windows geometries have defined the strict constraints that have been taken into account in the definition of the coating bench design. In this study, a full description of sputtering machine will be given.
By maintaining a constant bias and a fixed ionisation gas flow, an optimisation of reactive gas flow will be necessary for stoichiometric deposit obtaining. Once these parameters determined, a study of deposition rate variation for different process pressure value will be done. The influence of substrate to target distance on deposit stoichiometry and thickness will be also presented.
As TiN deposit thickness is a very important parameter to control, a correlation between quartz crystal microbalance given value and the real deposition thickness is determined for a better in-situ monitoring.

Chapter I:

Fundamentals and study's framework

I- Power coupler for superconductive cavities

Over the last few years, many different physics communities have shown a renewed interest in particle accelerator machines and particularly linacs. In fact, the request for increased machine performances, as far as the beam bunch length and the limits given by the synchrotron radiation are concerned, has to take into account the limitations imposed in the storage rings. Thus, new innovative concepts of linear machine are being developed worldwide, as example we name the energy recovery linacs (ERL) project, the proton high intensity machine and, last but not least, the international linear collider (ILC).

In these different frameworks, a common element is the utilisation of superconductive accelerating cavity technology. In fact, thanks to the recent significant increase in accelerating gradient, cold technology is considered suitable for high current and high gradient accelerators.

To provide power to superconductive cavities, special devises called RF power couplers are used. These last have to assure a good matching between the RF source (Klystron) and the cavities, in addition to an efficient separation between the two different volumes characteristics (air and vacuum) for the electromagnetic wave propagation (figure I-1).

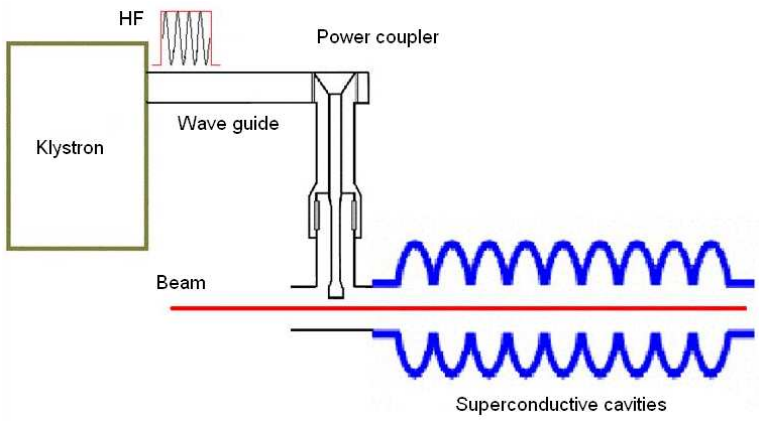

Figure I-1: *Coupler position in an accelerator power network.*
Presented coupler is a coaxial one allowing electrical coupling with cavities using an antenna.

I-1- Role of power coupler for superconductive cavities

Focusing on superconductive cavities operating conditions and strict constraint required to guarantee best performances and excellent preservation of beam characteristics, it become easy to deduce the roles that must fulfil an appropriate power coupler [1], [2].

I-1-1- Electromagnetic role

Power coupler basic function is to assure appropriate matching between RF power source and the cavity taking into account also the beam loading. An antenna is usually used to bring the delivered power into the cavity. Optimal coupling is obtained by an appropriate penetration of the antenna in the beam tube. However, this later operation can induce a dissymmetry in transversal electric field, and so the deviation of accelerated bunch. That's why a compromise should be found between those two constraints. If the constraints are limiting the use of a symmetric input, using two couplers, is taken into account to restablish the symmetry at least for the dipole mode.

Coupler must also guarantee a good impedance adaptation between RF power source and the cavity. Moreover, Ohmic loss in coupler should be minimised and an appropriate evacuation of the temperature from the internal part of the cavity has to be provided not to affect the superconductive state. For those reasons, internal coupler conducting surface are made of copper.

I-1-2- Vacuum barrier

Superconductive cavities are submitted to strict constraints of cleanliness and vacuum conditions that power coupler have to preserve. Ceramic windows are used to allow a good transmission of the electromagnetic wave without a critical temperature increasing but they play also the role of effective separation between the ultra high vacuum cavity environment from air (environment of the source). Windows can have different geometries depending on coupler design, they can be coaxial planar, planar, or cylindrical.

Those ceramic components are problematic devises because of their fragility and the additional industrial process- like brazing and thin film deposition- that they may need before

being a part of a coupler. Their positions into this later must be optimized to avoid very high fields at their location.

On another hand, as the coupler is a subject to pumping and HF excitation, it must not produce element that may contaminate cavities environment. Thus, an appropriate treatment of coupler internal surfaces should be planned.

I-1-3- Thermal interface

Superconductive state is hard to maintain during cavities functioning especially under high accelerating gradients. Consequently, the smallest extern or local thermal influence could let the cavities loose their superconductive state.

Cryogenic modules assure an efficient thermal isolation of cavities with the assumption that couplers are well designed and studied to guarantee a good isolation from ambient temperature medium. A cold region of the power coupler has to be taken into account as a fully integrated part of the cavity itself (Figure I-2).

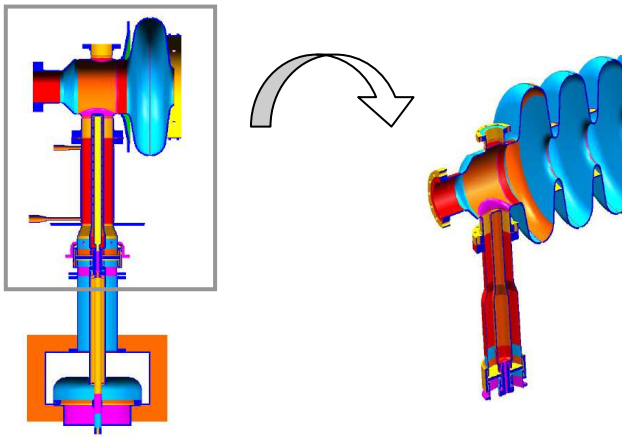

Figure I-2: *Coupler cold part integrated in cryogenic module as a fully part of superconductive cavities series*

As the power coupler is the interface between HF source (temperature of ~300K) and cavities (Cryogenic medium of ~1.8K), it must have an important thermal resistance to guarantee a high temperature gradient between its extremities and then avoid thermal flux transfer between the two mediums; hence the choice of stainless steel as a coupler basic material. At the time, as previously said, the copper plating must guarantee a good thermal evacuation of the cold part heating when RF power is injected in the cavity. So we face two requirements:

- a good thermal insulation to preserve the cavity temperature in static mode, i.e when there is not RF,

- a good thermal conductivity, to evacuate the heating given by the RF (dynamical mode).

All the thermal design is a careful process of equilibration of these two requirements to maximise the coupler performances.

Components materials choice and coupler geometry must be validated by a software simulation of mechanical stress caused by important temperature gradient. This allows avoiding some characteristics degradation, as adaptation to electromagnetic wave and sealing.

I-2- Power coupler design: example of TTF-III model

The significant increase in accelerating fields in superconductive cavities during the last years have induced new functional constrains. In order to propose new technological solutions, considerable efforts have been deployed in the study and conception of new coupler prototypes more and more reliable. To better illustrate the main parts of a coupler and their function we will provide in the following a concrete example. In Figure I-3, the TTF-III model is illustrated. This is the baseline solution for the future XFEL linac in DESY and for the ILC. This model choice is not trivial as it is one among other prototype we study in our laboratory.

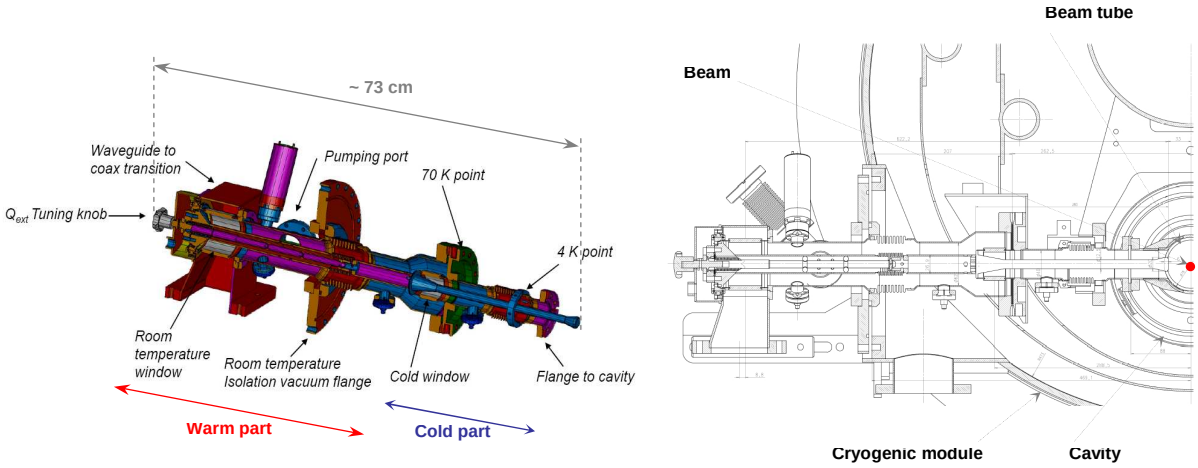

Figure I-3: *TTF-III coupler presentation and its integration in cryogenic module*

The observation of TTF-III coupler design allows the differentiation of three main functional parts.

I-2-1- Cold part

TTF-III coupler cold part is looking to the internal part of the SC cavity, sharing the same vacuum, in the beam line. A cylindrical ceramic window (cold window), placed at the input of this part, allows the limitation of the pumped volume shared with cavities, and all at once, permits a good propagation of Electromagnetic wave. In the extremity of cold part, a copper antenna permit power coupling in fundamental mode into the cavity.

Temperature in the cold part is regulated thanks to three thermalization points. The first one, localised near the cold window, have a temperature fixed at 70K, making a preliminary screen against thermal flux propagated essentially from warm part of the coupler. Thermal looses must not exceeds 6W at this level. The second point is maintained at 4K and presents a second protection against thermal transfer into the cavities that must be lower than 0.5W. the last point, localised at the flange in the extremity of this part is maintained at 1.8K, functional temperature of the cavities, The thermal power transfer in this point must be less than 0.06W [3], [4].

I-2-2- Warm part

TTF-III coupler warm part has a vacuum totally independent from the cold part. In fact, it is delimitated by the cold ceramic window and a similar other one (with larger diameter) called warm window, which makes an interface between the vacuum and the air. Unlike the cold part, the warm one is exposed to ambient temperature. It was designed to provide the needed gradient between external temperature and the one of the first thermalization point of cold part.

I-2-3- Wave guide transition

This part, totally on air, has essentially an electromagnetic role to play. It permits a progressive adaptation of the RF signal between wave guide network and warm part of the coupler. Some diagnostics could be performed thanks to measurement holes in the cupper box, like metal temperature control (PT100 detector), arc observation on warm window (arc detector), and temperature measurement on ceramic (IR detector).

The assembly of the wave guide transition and warm part must perfect in order to ovoid RF leak and bad contacts that could be at the origin of electric arc. This part is provided with a hole that permit introduction of a cooling gas in case of excessive heat of warm window.

I-3- Behaviour of coupler in HF power exposure

The behaviour of couplers submitted to RF power still very unpredictable. Their design complexity and their use for power increasingly high impose their studies in more and more constraining operational conditions. The difficulty of an exhaustive modelling of those devices requires the use of experimental methods allowing diagnostic of phenomenon that may happen during RF exposition and analysis of measurements obtained during this operation. The procedure called « coupler conditioning » is an essential step in preparation and treatment process of coupler after their fabrication and before their assembly with cavities [5]. It consists on a progressive increase of RF power delivered by the source to the coupler till reaching the maximum value that coupler has to provide to cavities in normal functioning.
This procedure permits coupler progressive adaptation to RF and evaluation of their performances, in addition to the monitoring and the study of its responses.

When the coupler is exposed to RF power in vacuum conditions, different physical phenomena may occur into it, and in some cases can cause significant damage. Among those phenomena we can cite:

I-3-1- Excessive electric field

Some welding and brazing imperfections can cause spikes on the surface. The latters will attract electrons causing an excessive electric field and generating energetic electron emission. This phenomenon is called the electron runaway effect.
In case of vacuum degradation, electric arc may occur causing a serious damage on power coupler surfaces by evaporation certain materials and thus contaminating the cavities, or worst, breaking the ceramic window and eliminate vacuum barrier.

1-3-2- Degassing

Surfaces excitation under vacuum condition by RF power can cause desorption of chemical entities trapped on coupler surfaces, which can contaminate cavities environment and may

decrease their performances. If the degassing is important, it can create conducive environment for arcing.

I-3-3- Multipacting

Multipactor discharges are considered detrimental to RF systems in most applications. The discharges can detune RF systems, limit the delivery of power, damage high power sources and cause a local pressure rise due to the desorption of surface face gases. In some cases [6], [7] multipactor can induce a glow discharge below the expected minimum pressure for a multipactor-free, Paschen-type RF glow discharge [8].
We will return in more details to this phenomenon in the following.

As we have just seen, all this phenomena are related to coupler internal surface state, excited by RF power. Thus, a particular attention must be paid at this subject in design and fabrication step as well as in treatment phase before assembling to cavities.

II- Coupler ceramic windows

According to what we have seen previously, ceramic windows are components of extreme importance in RF power coupler for superconductive cavities. They allow an excellent separation between air and ultra high vacuum mediums and a good RF wave adaptation in warm and cold part of power coupler (Fig. I-4).

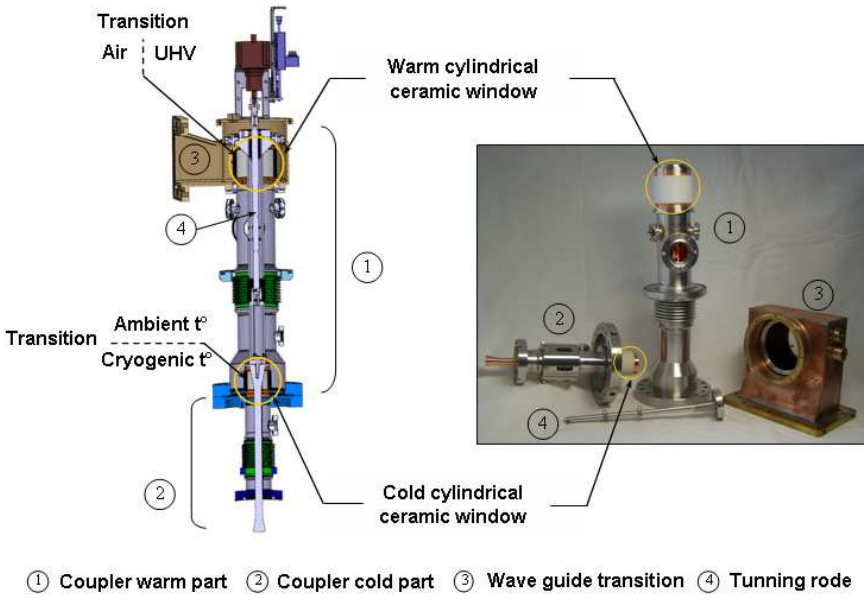

Figure I-4: *Location and role of ceramic windows in TTF-III power coupler*

Alumina (Al_2O_3) is a common material for RF windows. Besides its mechanical strength, it is stable under thermal treatment and has a low out-gazing rate [9]. Nevertheless, as we will explain in the following, some of its physical properties can cause problems when exposed to RF power. In addition, to be integrated to the coupler, a ceramic window must be brazed to copper, which will lead to the formation of metal-insulator interface called «triple junction», source of primary electron emission [10]. Figure I-5 show brazed ceramic windows of two different geometries.

Figure I-5: *TTF-III brazed cylindrical alumina coupler window (A), TW60 brazed disk alumina coupler window (B).*

II-1- Secondary electron emission yield

The Secondary Electron Emission Yield (SEY), denoted δ, expresses the faculty of a surface to emit electrons when exposed to a primary electron flux. It is function of the surface characteristics and of the primary electron energy. The typical dependence of the secondary electron emission yield as a function of the incident electron energy has usually the standard shape presented in figure I-6:

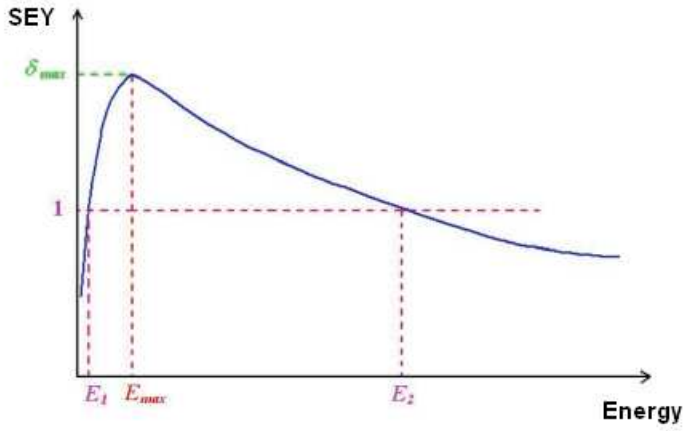

Figure I-6: *Standard shape curve of secondary electron emission as a function of incident electron energy.*

If the SEY varies depending on materials, the invariance of the shape is due to the fact that the principle is always the same: incident electron interact with a number of electrons, at superficial layer of the surface, proportional to its kinetic energy. When this later increases, incident electron penetration become very important and the electrons with which it interact will not be able to emerge and leave the surface.

When the value of δ is greater than 1, it means that more than one electron is ejected from the surface. This is one of the establishment conditions of multipactor phenomenon that we will introduce later. At the primary energy E_{max}, secondary electron production is at its maximal value δ_{max} and thus multipactor can be very intense. As multipactor is a harmful physical phenomenon for RF devises, it is important to note that it isn't the most energetic electrons that are the most nocuous.

To be back to alumina ceramic, we present in figure I-7 the secondary electron emission yield curve.

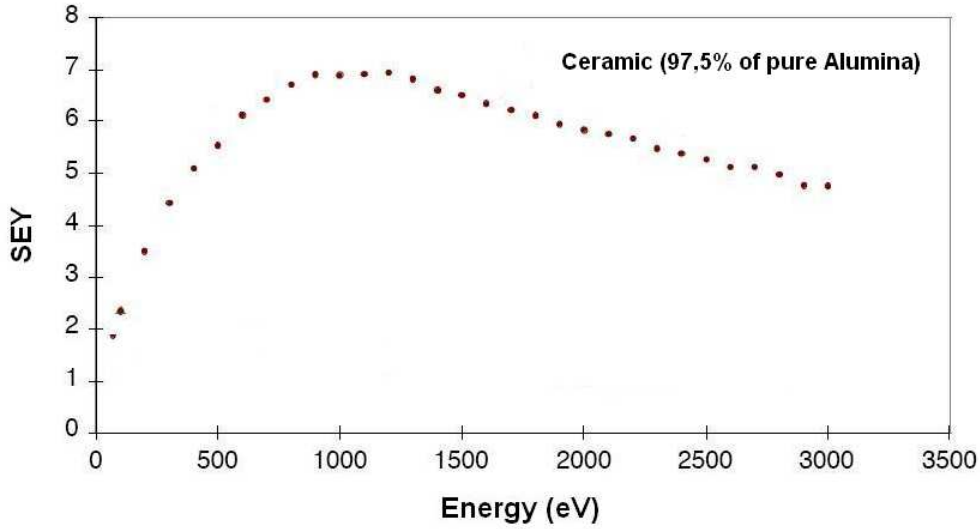

Figure I-7: *Secondary electron emission yield vs. energy for Alumina ceramic window.*

It is clear that for a wide energy range, SEY of Alumina ceramic is bigger than 1. This means that ceramic windows could be the site of intense multipactor activity if the other conditions are fulfilled.

II-2- Multipactor Phenomenon

II-2-1- Description of multipactor discharge

Multipactor effect is an electron-avalanche discharge that can occur on material surfaces exposed to RF electromagnetic fields in vacuum conditions.

This electron multiplication process occurs when an extracted electron gains energy from the alternating RF fields and strikes the surface with an impact energy in a range corresponding to a secondary electron emission yield, δ, greater than 1. Figure I-8 depicts a simplified picture of multipactor discharge.

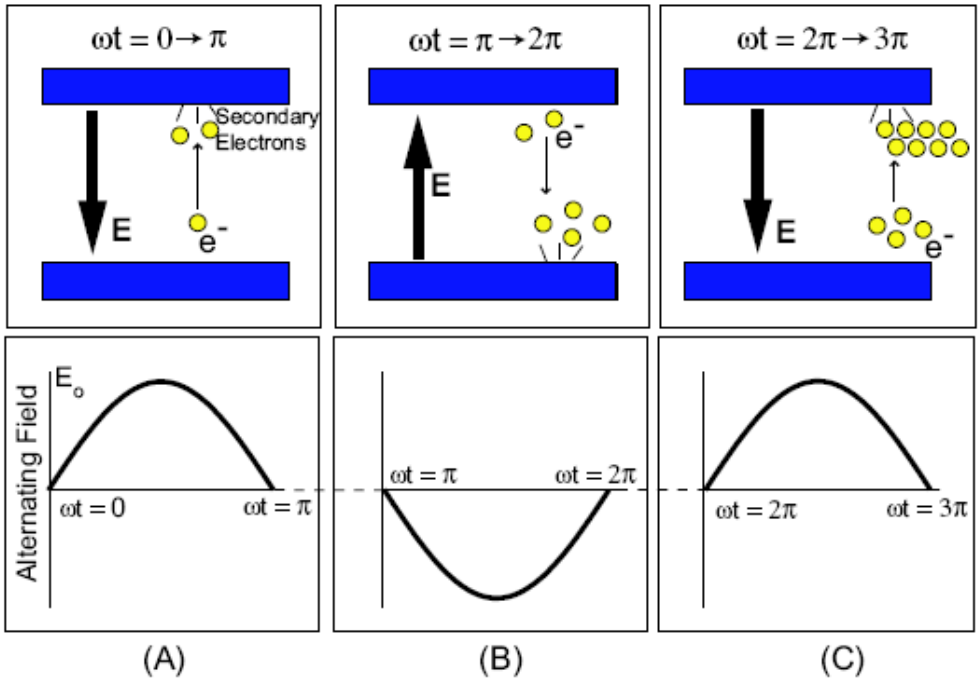

Figure I-8: *Simple explanation of a multipactor discharge with an electric field oscillating between two metal electrodes. Upon each electron impact, secondary electrons are emitted from the surface, multiplying the total number of electrons with each half cycle [11].*

In panel A, an electron is born and then accelerated by the oscillating electric field of the form $E_0 \sin(wt)$, with amplitude E_0, frequency w and time t. In this example, the electron hits the opposite electrode with sufficient energy for emission of two secondary electrons. This emission occurs near the time when the field reverses direction at $wt = \pi$, and these two secondary electrons, shown in panel B, are then accelerated across the gap in the reverse direction. Again, these electrons traverse the gap in half the cycle time and impact with enough energy to cause further electron multiplication by secondary emission. This process continues with each half cycle as the multipactor develops [11].

II-2-2- Conditions for multipactor establishment

The resonant electron motion described in Fig. I-8 relies on several factors for the successful development of the multipactor discharge.

First, the RF power and system geometry coupled with the accelerating electric field must give rise to this type of resonant electron motion; i.e. the electric field must be just right for a given frequency and geometry in order for electrons to impact the two surfaces in phase with the field. For example, if the electric field is too high for a given frequency and electrode spacing, the initial electron will impact too early, the secondary electrons will be emitted against the electric field, and they will not be able to accelerate back across the electrode gap.

On the contrary, if the electric field is too low, the electron may impact with insufficient energy for secondary electron emission. As a consequence, electrons which sustain the multipactor are focused into a narrow sheet over many cycles, impacting with the required phase range to sustain the resonance.

Secondly, the impacted surfaces must allow for a gain in the number of electrons by secondary emission. In fact, the secondary electron coefficient of material surface must be greater than unity for the incoming electron energy. The electrons of a pure multipactor discharge are supplied completely by secondary emission, so the secondary emission coefficient is critical to the development of the discharge.

Lastly, it is necessary for this discharge to occur under vacuum pressures, typically less than 1 mTorr [6], as frequent collisions with background gas can prevent the necessary resonant electron motion.

When the proper geometry, RF and voltage are combined in vacuum with surfaces possessing the necessary secondary electron emission characteristics, multipactor discharges can occur.

II-2-3- Mechanisms and order of multipactor

Two multipactor mechanisms are described in literature [12], [13]. The first one corresponds to impact points that are superposed, or that are close to the first impact point. In this case, electrons trajectory have nearly the same start point. This phenomenon is called a one-point multipactor. The second is characterized by electrons resonance between impact points belonging to two different plans. Electrons displacement will follow phase fluctuation of electromagnetic field established between the two surfaces. In this case, the phenomenon is called a two-point multipactor. Generally, we call an n-point multipactor the one that resonate between n impact plans.

Multipactor is also characterized by his order, defined for a one-point multipactor as complete oscillation period number of the electromagnetic field between electron emission instant and the first impact. In general manner, for n-point multipactor case, the order is defined as the total complete oscillation number during n impacts entire cycle. The lower multipactor order is the higher in its stability and the most harmful.

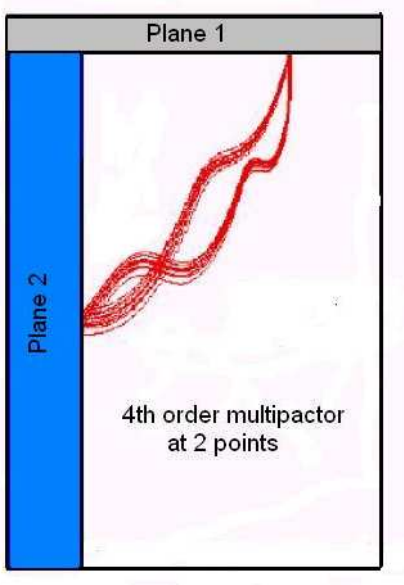

Figure I-9: *Representation of a 4th order two-point multipactor.*
Order is given by the oscillation number occurring in the space, so that an electron ejected from one point, come back to it after impacting one other point in an other surface [5].

II-2-4- Multipactor damages on Alumina windows

According to what we have just seen above, multipactor phenomenon can easily occurs in alumina ceramic due to the high SEY at all energy values. The results will be a sudden and drastic increase in the electronic current that can create damaging arcs that may lead to surface flashover, in addition a load mismatch causing dangerous reflected wave components to the RF source. The existence of «triple junction», due to ceramic-cupper brazing, makes the window more vulnerable because primary electron emission at this level causes accumulation of positive charge that may perturb electrical field. This effect, in addition of heating may lead to material evaporation an electrical breakdown effect.

III- Multipactor suppressor thin film

According to what we have seen previously, the presence of a ceramic window on a high power RF line has a strong influence on the multipactor phenomena. The only way to suppress, or at least attenuate this effect is to decrease the secondary electron emission yield of this device by coating its surface with a thin layer of a material having a low SEY.

Several thin film coatings like Cr, CrN, TiCr [25], Cr_20_3 [24, 27], Diamond Like Carbon (DLC) [10], Ti [27] and TiN [9, 10, 24, 26, 27], were used for this purpose. The aim was to reduce the multipactor and to confer a long-term stability to the surface under operating conditions. Among these materials,

TiN is the most appropriate material, widely used not only for coupler ceramic window coating [9, 26], but also for most RF devices that can be subject to multipactor occurring [23, 24, 27, 28].
In fact, beside its excellent mechanic properties (high hardness, good wear and corrosion resistance), TiN is characterised by a low SEY that remains stable on RF operational conditions. This criterion makes it the most reliable multipactor suppressor used in RF devices. To show the efficiency of this material, we show in Figure I-10 a superposition of secondary emission yield for TiN coated and uncoated ceramic window.

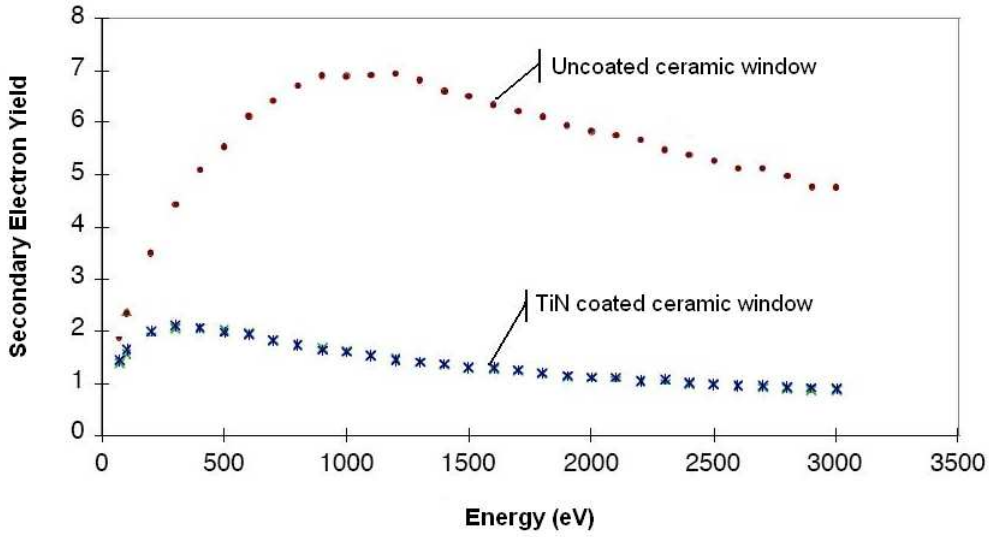

Figure I-10: *Influence of TiN coating in Secondary electron emission yield decrease*

The difficulty with TiN is to catch the right stoichiometry. In fact, several nitride compound of titanium (TiN_x) can be obtained if the coating process is not well optimised. This difference of composition can induce a change in film properties. Various methods have been employed for TiN deposition [26, 29-32], among them reactive sputtering technique (DC and RF). The importance of sputtering methods is that they involve a number of parameters that allow different combinations for a high quality films obtaining with required properties.
In our case DC reactive magnetron sputtering will be chosen for TiN deposition *(§I- IV- DC reactive magnetron sputtering).*
Some precisions have to be, however, done concerning our deposit. Operational conditions in RF field induce some additional constrains in our deposit characteristics. In addition to stoichiometry, film thickness has to be optimised for a good functioning condition of the ceramic window. In fact, deposited layer should be thick enough to reduce multipactor effect, but not so much to prevent increasing RF power reflection in ceramic surface because of its properties modifications. According to Lorkiewicz et al. [26], a range of 7-15 nm thickness has been found a good compromise between these contradictory requirements.

III- DC reactive magnetron sputtering

Before presenting this technique, let's describe briefly the basic sputtering process that is at the origin of many deposition derived techniques.

III-1- Basics of sputtering deposition

Sputtering is a conceptually simple technique: a target made of the material to depose is bombarded by energetic cations, attracted by the target negatively biased. When the cations strike the target they dislodge its atoms and sputter them off. The dislodged atoms having substantial kinetic energies will fly to the substrate to be coated and stick there.

In figure I-11 we present the basic set up of sputtering process:

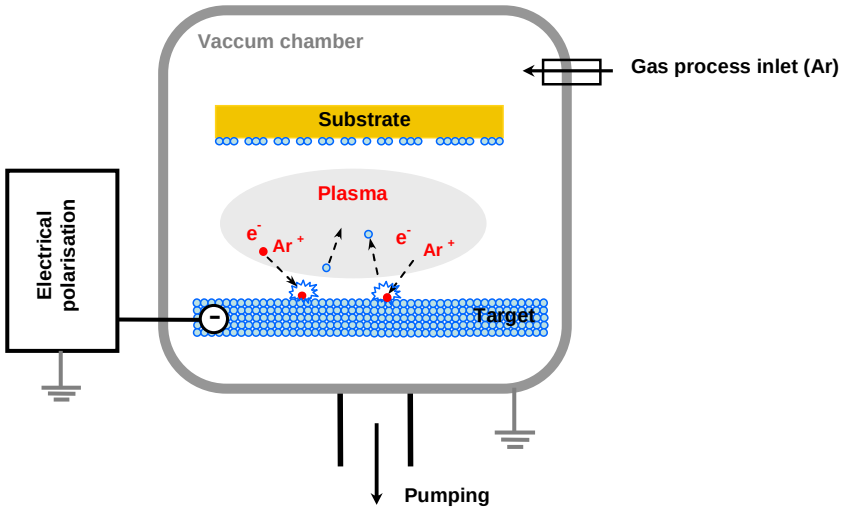

Figure I-11: *Principle of DC sputtering deposition*

The ions necessary of the bombardment of the target are extracted from an argon plasma (ionized Ar and free electrons forming a global neutral medium) burning between the target and the substrate. The argon, called gas process or ionisation gas, is introduced to the vacuum chamber after a pumping until a base pressure of 10^{-6}-10^{-7} mbar to eliminate residual gases that may perturb the process.

Some target atoms sputtered will be coated at the substrate, other will miss it. The first category will hit the substrate with an energy large enough so they "get stuck", but not so large to liberate substrate atoms. Sputtered layers therefore usually stick well to the substrate and homogeneous coverage is easy to achieve.

The sputter process has almost no restrictions in the target materials, ranging from pure metals were DC (direct current) power supply can be used, to semiconductors and insulators which require a RF (radio frequency) power supply or pulsed DC.

One derived technique from the basic method is the magnetron sputtering. It involves placing a magnet behind the target, thus during the sputter process a magnetic field can be used to trap secondary electrons close to the target. The recombination of electric and magnetic fields let the electrons follow helical paths around the magnetic field lines undergoing more ionizing collisions with neutral gaseous near the target than would otherwise occur. This enhances the ionisation of the plasma near the target leading to a higher sputter rate. It also means that the plasma can be sustained at a lower pressure. The sputtered atoms are neutrally charged and so are unaffected by the magnetic trap.

III-2- Basics of reactive sputtering

III-2-1- interest and advantages

Reactive sputtering can be defined as the sputtering of elemental targets in the presence of chemically reactive gases that react with both the ejected target material and the target surface. It has become a very popular technique in today's search for new material properties, for the deposition of a very wide range of compound and alloy thin films including oxides, nitrides, carbides or fluorides [14].

Besides the improved properties of non-reactively sputtered films, the popularity of DC reactive sputtering from elemental targets (i.e. a target consists of a single element) can be attributed to several factors, among them:

i. It is capable of producing thin compound films of controllable stoichiometry [15] at high deposition rates and on an industrial scale [16], [17].
ii. Elemental targets are usually more easily purified, and hence, high-purity films can be produced [18]
iii. The complexity and expense of RF systems can be avoided since metallic targets are generally electrically conductive, and hence, DC power can be applied
iv. Elemental targets are usually easy to machine and bond
v. Metallic targets are thermally conductive, which makes the cooling of these targets more efficient. Thus, the range of the applied power can be extended without the fear of being cracked

vi. Films are deposited at temperatures less than 300°C.

Figure I-12 shows the basic DC reactive magnetron sputtering:

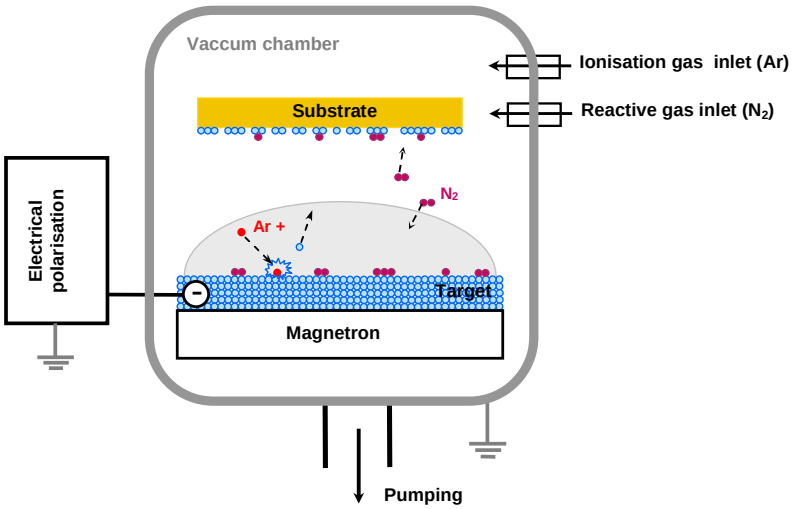

Figure I-12: *Principle of DC reactive magnetron sputtering*

Although reactive sputtering is conceptually not so different from the basic method described previously, it is in fact a complex non-linear process which involves many interdependent parameters. The presence of the reactive gas at both the cathode surface and the substrate results in strong interactions of the reactive gas not only with the condensing material but also with the cathode surface, causing the so-called target poisoning. To better understand the principle on reactive sputtering, we should explain the later phenomenon.

III-2-2- Target poisoning and hysteresis effect

First, we should precise that reactions in the gas phase, between reactive gas and sputtered target atoms, are ruled out for the same reasons that ions cannot be neutralised in the gas phase (there is no mechanism which can dissipate the heat of neutralisation to conserve both momentum and energy in a two-body system, therefore it can only happen at a surface).

The target reactions are seen to occur suddenly at some rate of reactive gas flow. If the flow control of reactive gas is used, such reactions are marked by a change in the impedance of the operating plasma, an abrupt increase in the system pressure (or more precisely, in the reactive gas pressure), a drastic drop in the deposition rate and a change in the film from metal-rich to gas-rich (i.e. a change in the stoichiometry). Figure I-13 resumes all this effects.

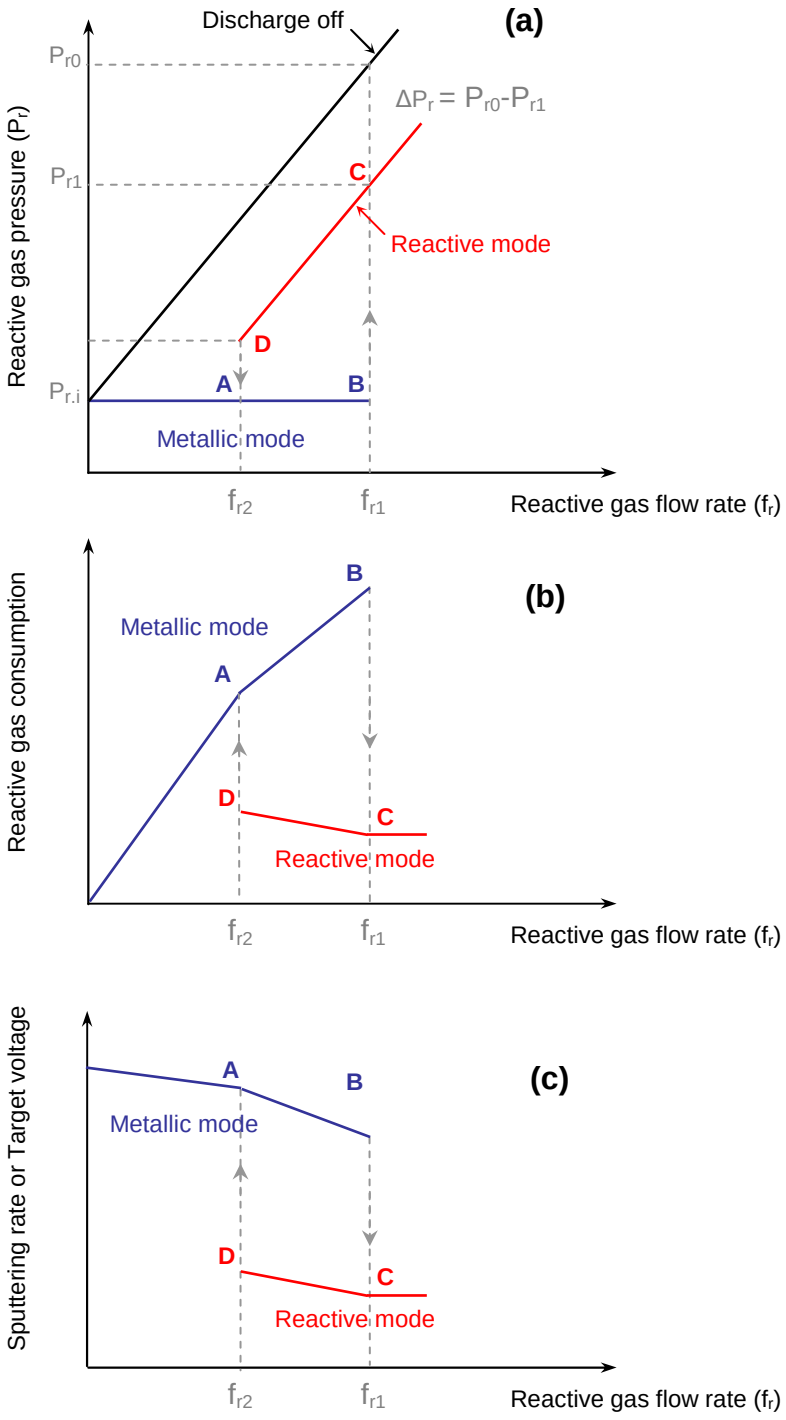

Figure I-13: *The hysteresis behaviour of reactive sputtering.*
(a) Hysteresis behaviour of reactive gas pressure. (b) Hysteresis behaviour of reactive gas consumption.
(c) Hysteresis behaviour of sputtering rate or target voltage.

Fig. I-13 (a) shows schematically the well-known and important feature of reactive sputtering at a constant partial pressure of non-reactive gas, when flow control of reactive gas is employed: a hysteresis curve of the reactive gas partial pressure, P_r, as a function of the

reactive gas flow rate, f_r, at a constant sputtering power (or as a function of sputtering power at a constant reactive gas flow rate). At low values of f_r (e.g. point A in Fig. I-13 (a)), almost all the available reactive gas is gettered at the condensation sites. As a result, no essential change in P_r is observed from the background level and the deposited film is metal-rich. This situation prevails until f_r reaches a critical value, f_{r1} (point B in Fig. I-13 (a)), where the flow rate of the reactive gas into the chamber becomes higher than the gettering rate of the sputtered metal. The reactive gas reacts, then, with the target surface to form a layer of the gas–metal compound. Sputtering rates from compound targets are less than that of pure metallic targets by a factor of 10–20, for mainly two reasons:

- the sputtering yield of metal atoms from a compound on the target surface is less than that from a pure metallic target;
- compounds have higher secondary electron emission coefficients than metals and hence most of the energy of the incident ions is utilised to breaking bonds with the resultant creation and acceleration of secondary electrons.

Consequently, less metal atoms are sputtered and less reactive gas is consumed in the reaction, and a sudden and sharp rise in the reactive gas partial pressure to a new value, P_{r1}, occurs (point C in Fig. I-13 (a)). The deposited film is then gas-rich. If f_r is reduced following an increase in P_r to a high level, P_r will not decrease following the same trajectory as it increased. ΔP_r will stay constant until some value f_{r2} (point D in Fig. I-13 (a)) where it abruptly increases and the reactive gas pressure decreases to the background level. This is because the reactive gas pressure remains high until the compound layer on the surface of the target is removed and metal is exposed to be sputtered once more. As a result, the consumption of the reactive gas increases and the deposited film is metal-rich again. The dependence of both reactive gas consumption and deposition rate on reactive gas flow rate are seen in Fig. I-13 (b), (c), respectively.

The hysteresis effect is very undesirable and has to be eliminated, if the flow control of reactive gas is used, because the process is unstable inside this region [18]. At one value of f_r, it is likely to deposit compound films of different stoichiometries and thus physical properties. This is due to the existence of two stable operating states corresponding to an individual value of f_r, when f_r is in the region of hysteresis. Fast and sophisticated process control systems are required in order to operate inside this region.

All the above discussion has been related to DC sputtering systems, which are characterised by a uniform plasma density across the target surface. This is not the case in magnetron cathodes, in which the plasma is highly localised in the racetrack region leading to an inhomogeneous discharge current density across the cathode. As a result, poisoning of the target must be site-dependent leading to the possibility of a simultaneous existence of three states on the target surface: fully metal, fully poisoned or partially poisoned [19].

Despite the differential poisoning at a given reactive pressure, the hysteresis effect was also observed in magnetron cathodes [20-22].

Chapter II:

Titanium nitride sputtering system

I- Specifications of the coating system

Coupler operating conditions, physical properties of TiN coating layer and alumina substrate, and ceramic windows geometries have resulted on strict constraints that should be taken into account when defining the sputtering system design. Required technical specifications are presented in the following.

I-1- General requirements

Sputtering system should allow the deposition of TiN layers which thicknesses could vary from a very thin deposit (some nanometers) where the material doesn't drain away electric charges, to a thick deposit (some hundred of nanometers) where the material conductivity reduces power transfer and causes material heating.

Concerning deposition on ceramics, two different treatments are needed. The first one should be on the inside and outside faces of ceramic cylinders, the second should be on the bottom and top grooves of ceramic cylinders (where the brazing with cupper is carried out). The deposits on grooves should be thicker than the one on faces because of the vulnerability of windows at triple junction (*§-I, II-2- Multipactor phenomenon*).

For disk ceramic, both side of the disk should be coated. It could be also useful to determine if a simple deposition of pure Ti instead of TiN can work.

I-2- Deposit quality

The sputtering system has to be able to coat a very thin layer of TiN on disk and cylindrical ceramic with a minimum quantity of oxygen (<3%) and the thickness has to be precisely adjustable in a range between 5 and 40 nm. Furthermore, the machine has to be enough efficient to reproduce with the same parameters, a same deposit thickness at ±25%.

On a cylindrical window, the minimum fixed deposition thickness will be assumed as equal to the setting defined as the thickness at the half-height of the ceramic cylinders. On the other hand, the maximum limit of deposition thickness will be twice the setting one.

It is clear that window geometries provide not only the coating difficulty, as described above, but also the way to hold it during the process. That's why we tolerate having windows (cylinder and disk) with three non-coated point that allows to introduce a holder.
It is worth recalling that deposits must show excellent sticking properties on ceramic (97.5% of pure alumina).

I-3- Pumps, vacuum chamber and vacuum control system

Due to the drastic cleanliness constraints applied to all coupler devices, the machine has to have an oil free pumping system that allows reaching a pressure of 10^{-7} mbar. If dangerous gases have to be used in the process, other pumps have to transfer pumped vapours outside the room. Each gas entrances have to be installed with filters. These one have to be fixed as close as possible to the vacuum chamber. A Nitrogen (99.999% pure) entrance has to be designed for vacuum breaking.
The vacuum chamber and pieces going inside it have to be made only of:

- 316L stainless steel.
- Copper for UHV
- Cu-Be: beryllium copper
- Pure titanium and titanium nitride
- Aluminium
- Ceramics

All flanges have to be foreseen as CF flanges with metallic seals. Only ceramic window entrance porthole (usually disassembled) can use elastomer/rubber seals with low permeation and that can be heated until 400°C. One or two glass portholes should be available in vacuum chamber in order to visualise and control process when occurring. Otherwise, to improve the machine in the future, 1 or 2 portholes should be available.
A system will measure the vacuum from atmospheric pressure to 10^{-7} mbar; this will be doubled if it's necessary. A porthole will be reserved for a gas analysis system

I-4- Process and controls

During all the process, the following parameters should be recorded using the appropriate instruments:

- Time
- Vacuum chamber pressure

- Gas flows
- Electric Intensity and voltage
- Deposit thickness fixed

All the data from these systems and the control parameters must be recorded during the process. A storage data system has to be included in the machine. More over, we should be able to transfer all data from the machine to a laptop. As this equipment is designed for R&D activities, the machine has to be flexible, in particular on “control parameters”, on gas lines and on the shape/size of treated pieces. A maximum of machine parameters must be variable.

II- Sputtering system description

The conception and the development of the sputtering system that we will describe in the following were made in collaboration with the team of Superconductivity Laboratory at Legnaro National Laboratory in Italy.
Vacuum chamber, magnets and sample holder, that are important devices of the systems were totally designed and developed in Legnaro laboratory.

II-1- Pumping and vacuum control system

To eliminate the risk of sputtering machine contamination, the machine has been designed having an oil free pumping system. It consists of a primary Triscroll pump and a high vacuum turbomolecular one. It allows reaching a base pressure of 10^{-7} mbar.
Ionization and capacitive vacuum gauges are used to control respectively base pressure before deposition and process pressure when ionisation and reactive gases are introduced. Another Pirani gauge is placed between primary and turbo pump to order the aperture of valve situated at the same place assuring a good function of pumping system.

II-2- Vacuum chamber

The vacuum chamber is made of AISI 316 stainless steel. It is flanged with two CF 150 standard flanges positioned symmetrically, and eight CF 35 standard flanges (Figure II-1).

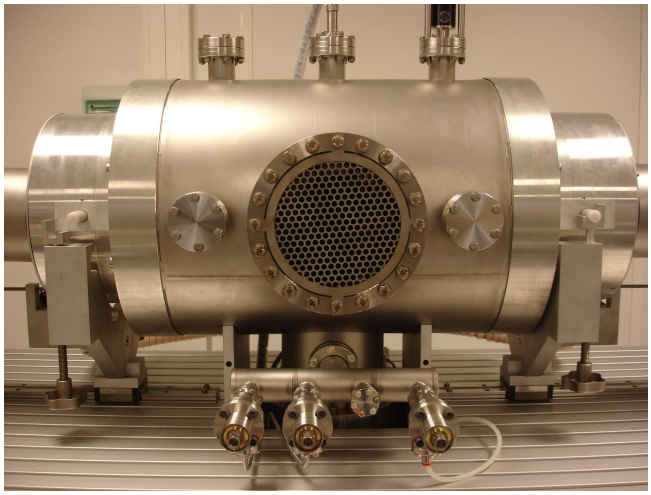

Figure II-1: *Vacuum chamber of sputtering machine*

All flanges with a low probability to be disassembled like pumps, instrumentation etc..., have been foreseen as CF flanges with metallic seals, while only the coupler windows entrance porthole, magnetrons and the UHV gate valve can use rubber seals.

All gas entrances (Gas process (Argon 99.999% pure), reactive gas (Nitrogen 99.999% pure) and gas for venting (Nitrogen 99.999% pure)) have been designed with filters filtering particles with a diameter bigger than 0.2 µm and the filters have been inserted as close as possible to the chamber. Three all metals valves placed on the front part of the vacuum chamber are connected to those gas lines.

The device parts that constitute the internal part of the vacuum chamber have been made of 316L stainless steel, Copper for UHV, Cu-Be beryllium copper pure titanium and titanium nitride and ceramics.

II-3- Targets and magnet packs

In the both sides of vacuum chamber, the machine is equipped with a 10 inch titanium disc target (Figure II-2 (A)) of high quality (grade 2, minimum 99.7 % Ti). A rotary magnet pack is placed just behind each target. The set is provided with a shield installed on a rail to facilitate its displacement when introducing samples to be coated. Special shape rotating magnets are used not only to increase plasma density at target surfaces and thus ameliorate sputtering yield, but also to delete target poisoning phenomenon (Figure II-2 (B)).

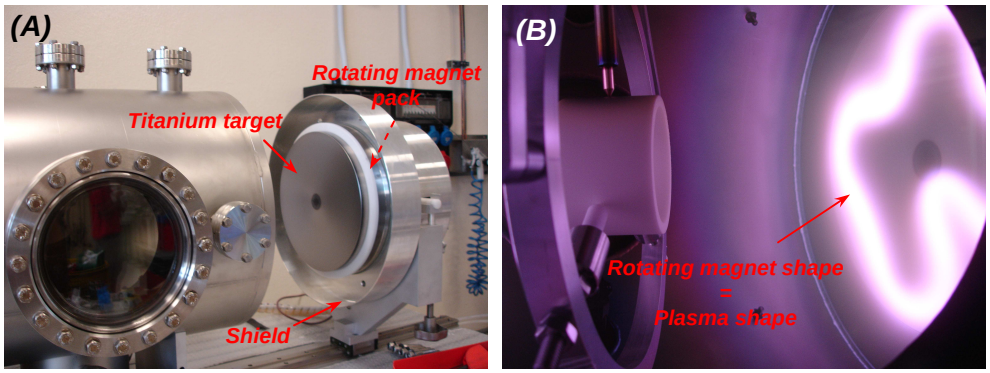

Figure II-2: *Components of sputtering machine*
(A) Titanium disc Target, magnet pack and shield; (B) Plasma confinement in target surface by rotary magnetron;

The 10 inch magnetrons are water cooled. Cooling circuit of every target is controlled in an independent mode with taps. An automatically shuts off occur in case of overheating.

II-4- Sample holder

The sputtering is done by two oppositely faced planar magnetrons. Each one of them contains a rotating magnet pack that confines the plasma in a rotating strip on the pure titanium targets. A special three tips sample holder permit to fix cylindrical (also disk) windows (Figure II-3).

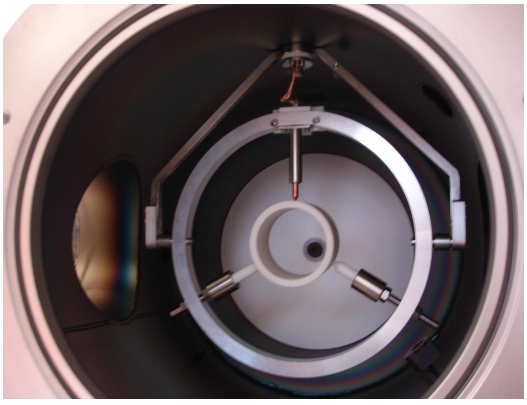

Figure II-3: *Three tips sample holder for cylindrical and disk samples*
The two lower rods are adjustable to fit to sample dimension, the top rod in copper is exchangeable, three length are available, to have always a centred sample.

The device is designed to work with three types of cylindrical (or disk) samples with external diameters of 47mm, 62.6mm, and 75mm respectively.

In order to guarantee a more uniform film thickness distribution, the sample holder is moved in a precession motion about its axis of rotation with a tilt angle of about 25° and a speed range of 0-20 rpm. Figure II-4 show different sample holder system constituents that allow its motion.

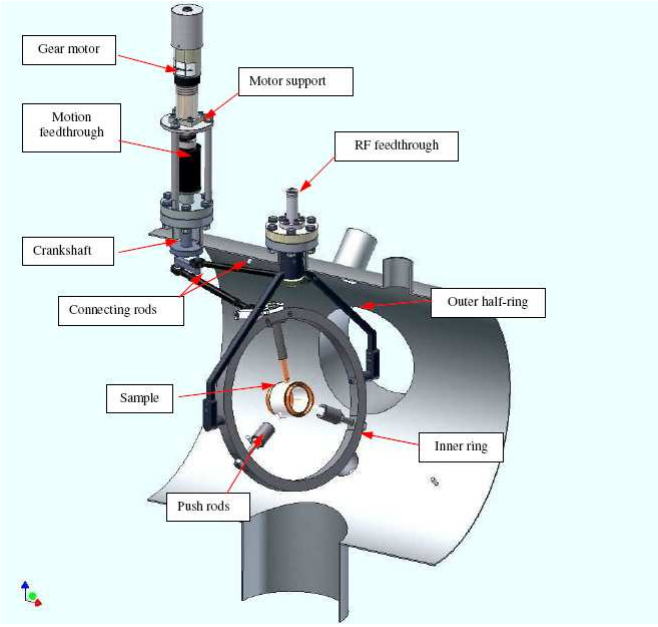

Figure II-4: *Section view of the vacuum chamber with the sample holder system constituents*

The sample holder is composed of the following parts:

- a gear motor, external to the vacuum chamber, supplied by 24VDC;
- a standard vacuum rotary motion feedthrough mounted on a lateral CF flange;
- a standard RF feedthrough mounted in the central CF flange;
- a gyroscopic holder, internal to the vacuum chamber, which delivers the precession motion to sample. It is composed of an outer half-ring, an inner ring, connecting rods, push rods to hold the sample and copper wire to transmit RF power on it.

In addition to his function of rotating sample holder, this device is also designed to provide RF power to the samples creating a discharge at its surface. As it is not possible to clean ceramic with solvent due to the high porosity of the material and the possibility of solvent trapping, Plasma cleaning of the surface permit to remove dust and other contamination that can affect TiN thin film adhesion on ceramic (Figure II-4).

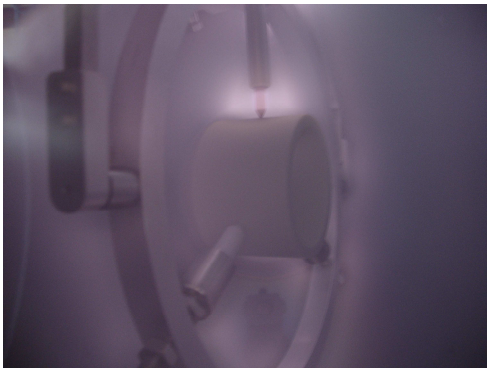

Figure II-4: *Plasma cleaning process- RF power matching thanks to cupper rod.*

II-5- Front panel: controls and racks

The front panel system is divided to three parts containing controls and modules installed in racks as it is shown below in Figure II-5.

The top of the left part contains an emergency shut off, a power supply switch for the entire system, in addition to switches for gear motors (sample holder and magnetrons). Each of the magnetron is piloted by a power supply placed in its side. It allows varying the bias value acting on current, tension, or power.

As the coating thickness optimisation is an important point to consider, a crystal quartz microbalance integrated to the bench allows following the deposit thickness and the deposition rate during the process.

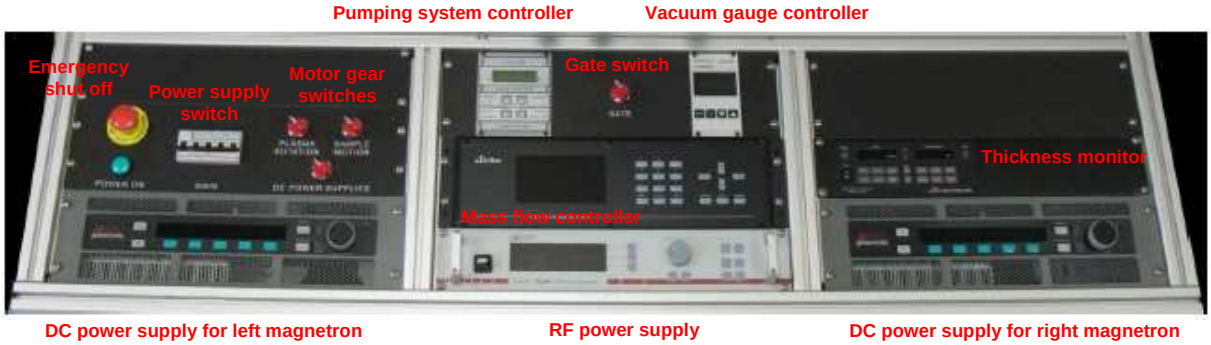

Figure II-5: *Front view of the control panel*

In order to obtain a stoechiometric TiN, reactive sputtering process needs the optimisation of gas and electrical parameters. Thus, the bench includes a mass flow controller for gas process (Argon) and reactive gas (Nitrogen). This device permits also following the process pressure measured by capacitive gauge. Another vacuum gauge controller in the central part of the

panel allows following base pressure measured in the chamber by Bayard-Alpert ionisation gauge. This part contains also an RF power supply for ceramic plasma cleaning process.

A switch in the top side of this part commends opening and closing of a pneumatic valve separating vacuum chamber from pumping system. This later is commanded thanks to the controller placed in this same part of the panel.

Figure II-6 present a sputtering machine overview:

Figure II-6: *Magnetron sputtering system overviews.*

Chapter III:

Results and discussions

I- Practical guidance's

During this practical part of the study, we will focus in two important characteristics of the deposited films: their stoichiometry and their thickness.
If it seems clear that the stoichiometry is the basic parameter to monitor in order to get multipactor suppressor property of the film, the optimization of the thickness still an operational requirement. In fact, a too thick coating will increase the HF reflection coefficient on the ceramic window while a too thin one will loose its multipactor suppressor characteristics. XRD analysis will be used for stoichiometry determination and control, while reflectivity and quartz crystal microbalance will be used for thickness setting and control.

In all parameter optimisation steps that will follow, deposits will be made on 10x10 mm quartz substrates, unless further precision. These latters are more suitable than alumina substrates for XRD and reflectivity analysis that will be performed. Furthermore, since the substrate number used is quite high, the cost will be much more advantageous than when using alumina ceramic substrate.

For sample characterisations, some limitations are imposed by the technique to perform. In fact, for XRD analysis the sample should be thick enough (some hundred of nanometers) to be characterised, while in reflectivity analysis, layer thickness can not be measured if it exceeds one hundred nanometer. Thus, the deposit thickness will be adapted to the analysis to carry.

Some experiments that will be presented later need a special sample holder different from the one described in the previous chapter. We will precise and present when needed the sample holder used.

II- Parameters optimization for a stoichiometric deposit

As it was described previously *(§-I, VI-2- Basics of reactive sputtering)*, titanium nitride deposit is obtained by reaction of reactive gas (N_2) with sputtered titanium atom on substrate surface. However, this reaction can lead to a non-stoichiometric deposit TiN_x ($x \neq 1$) if reactive gas flow rate is not optimized for a given bias and ionisation gas flow rate.

To perform this optimization step, and taking into account the great number of TiN_x film to deposit before obtaining the right parameters, a special multi-sample holder was designed allowing the introduction in vacuum chamber of seven couple of samples at the same time (Figure III-1).

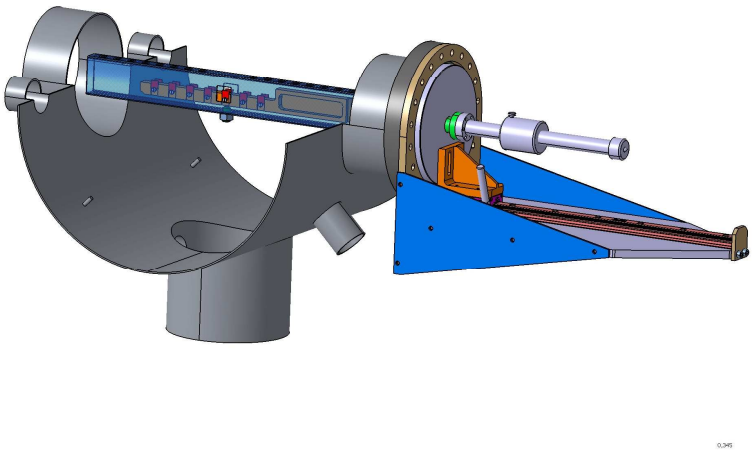

Figure III-1: *Section view of the vacuum chamber with the multi-sample holder*

For an imposed current I=3A, and by maintaining the Ar flow rate constant at f_{Ar} = 0.1 sccm, several TiN_x layers of ~ 500 nm were deposited for different values of N_2 flow rate. XRD analyses are performed to control film stoichiometry. From the plot $I_r = f(2\theta)$ (where I_r is the relative intensity of diffracted X-ray and 2θ is the angle between X-ray source, substrate and detector), it is possible to determine spacing between the planes in the atomic lattice d_{hkl} by applying Bragg's law:

$$d_{hkl} = \frac{n\lambda}{2\sin\theta} \qquad (III\text{-}1)$$

(Where λ is the wave length of x-ray source, in this case we have a Cu tube with a λ of 1.54056Å).

Then, it is possible to calculate the lattice parameter for each deposit, assuming that TiN_x crystallizes in a face centred cubic system using the relation:

$$a_{TiN_x} = d_{hkl}\sqrt{h^2+k^2+l^2} \qquad (III\text{-}2)$$

(Where (hkl) are Miller indices for diffraction plane)

From the obtained value of the lattice parameter, it is possible to calculate *x*, the N/Ti ratio, according to the relation below, valid in the range $0.6 < x < 1$ [36]:

$$a_{TiN_x} = 4.1925 + 0.0467\,x \qquad (III\text{-}3)$$

Figure III-2 shows XRD patterns for some TiN_x layers obtained according to the protocol cited below.

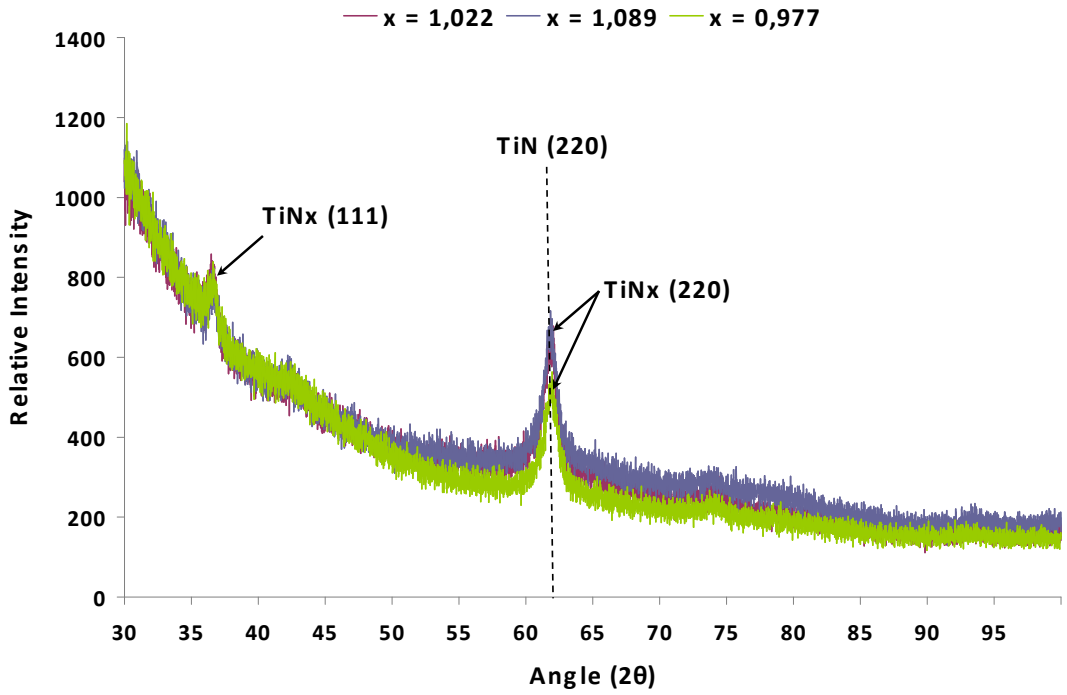

Figure III-2: *XRD plot for different TiN_x deposits compared to stoichiometric film.*

All diffraction curve presented above show two peaks corresponding respectively to the plan (111) and (220), indicating a high preferential orientation of the deposed films, especially in (220) direction. Considering the sharp and relatively intense peak corresponding to this direction, we calculate x, the N/Ti ratio, for different deposed TiN_x films according to the method cited previously.

The table III-1 summarizes the results obtained:

Table III-1: *lattices parameter and correspondent stoichiometry of deposits at different N_2 flow rate.*

Ar (sccm)	N2 (sccm)	I (A)	2θ	d (220) (Å)	a (Å)	x(TiNx)
0,10	0,11	3	61,8629	1,50115	4,2459	1,1423
0,10	0,12	3	61,8430	1,50028	4,2434	1,0896
0,10	0,13	3	61,8938	1,49917	4,2403	1,0223
0,10	0,14	3	61,9277	1,49843	4,2382	0,9775
0,10	0,15	3	62,1270	1,49410	4,2260	0,7153

As we can see, stoichiometric films are obtained for a N_2 flow rate between 0.13 and 0.14 sccm for a fixed Ar flow rate of 0.1 sccm and an imposed current of 3A. We should precise that the results shown in the previous table are just a selection among many attempts of stoichiometry obtaining. We choose to present these one because they seem interesting to study.

Observing the results on the table III-1, we note that increasing nitrogen flow causes the decrease of TiN lattice parameter, and consequently *x* the N/Ti ratio according to Eq (III-3).

This behaviour seems to contradict what was expected. In fact, according to the theory *(§I- III-2-2- Target poisoning and hysteresis effect)*, an increase of nitrogen flow rate should increase the N/Ti ratio till reaching the stoichiometry; such results were obtained by Hugen et al. [33].

The behaviour difference of our experiments is due to the fact that we are already in sub-stoichiometric conditions. Thus, a further increase of nitrogen flow rate acts more on increasing poisoning phenomenon, and thus modifying process pressure and deposition rate, than modifying the film stoichiometry. A similar behaviour was reported by Huang and co-workers [35].

Concerning the little variation in sub-stoichiometric conditions, several studies have found that the phase can have a significantly greater lattice parameter that can reach 4.3 Å [37] (although than 4.24 Å). To explain this lattice expansion, it was assumed that two factors can be responsible. One is nitrogen entrapment in non equilibrium positions during film growth. The second is internal macrostrains [35]. The first assumption could be supported by the measurements of deposition rate and process pressure illustrated in table III-2:

Table III-2: *Process pressure and deposition rate variations with nitrogen flow rate*

Ar flow rate (sccm)	N2 folw rate (sccm)	Process pressure (mbar)	Deposition rate (Å s-1)
0.1	0.11	8 10-3	3.2
0.1	0.12	8 10-3	3.1
0.1	0.13	9.33 10-3	3.0
0.1	0.14	9.33 10-3	2.9
0.1	0.15	10.66 10-3	2.7

For the lowest N_2 flow rate, deposition rate is the highest; this may be favourable for nitrogen entrapment on non equilibrium site. As the N_2 flow rate increases, process pressure slightly increase and deposition rate decrease; the reactive reaction between titanium and nitrogen become more stable and stoichiometry is reached. A further increase in reactive gas flow rate causes further change in process pressure and deposition rate, which means that poisoning effect still going on leading to new operational conditions that may lead to a film composition totally different. This may explain the drastic change in stoichiometry for lat measurement of table III-2.

III- Deposition rate variation with process pressure

Deposition rate is a very important parameter to consider in so far as it can influence the film morphology, its physical and mechanical properties, and even chemical composition since a low deposition rate of TiN could increase its oxidation.

In our case, in addition to the cited reasons, the choice of deposition rate is also an operating criterion. In fact, as we need to deposit some nanometers of stoichiometric TiN, we should choose the appropriate value so that the process occurs in a reasonable time in a good process conditions.

Once the stoichiometric parameters are reached by determining the appropriate N_2 flow rate value for a fixed value of Ar flow rate and an imposed bias (f_{Ar} = 0.1 sccm, f_{N2} = 0.14 sccm, I = 3A), we will now vary the flow rate for both gases keeping the ratio relative to stoichiometric conditions (f_{Ar} / f_{N2} = 0.71). The aim is to vary process pressure without modifying stoichiometric conditions and see the influence of such variation on deposition rate. Results are summarized in the following table:

Table III-3: *Deposition rate variation with process pressure at stoichiometric conditions of gases flow rate.*

Ar flow rate (sccm)	N2 folw rate (sccm)	Process pressure (mbar)	Deposition rate (Å s-1)
0.060	0.084	1.33 10-3	4.7
0.070	0.098	2.66 10-3	4.4
0.080	0.112	4.00 10-3	3.8
0.090	0.126	6.66 10-3	3.4
0.100	0.140	8.00 10-3	3.1
0.110	0.154	9.33 10-3	2.8
0.120	0.168	1.06 10-2	2.5
0.130	0.182	1.19 10-2	2.2
0.140	0.196	1.33 10-2	2.0
0.150	0.210	1.46 10-2	1.8

Before commenting the previous results, we show in figure III-3, XRD plots of two TiN deposits made at different flow rate of argon and nitrogen, but with respect of the ratio of stoichiometric conditions (f_{Ar} / f_{N2} = 0.71):

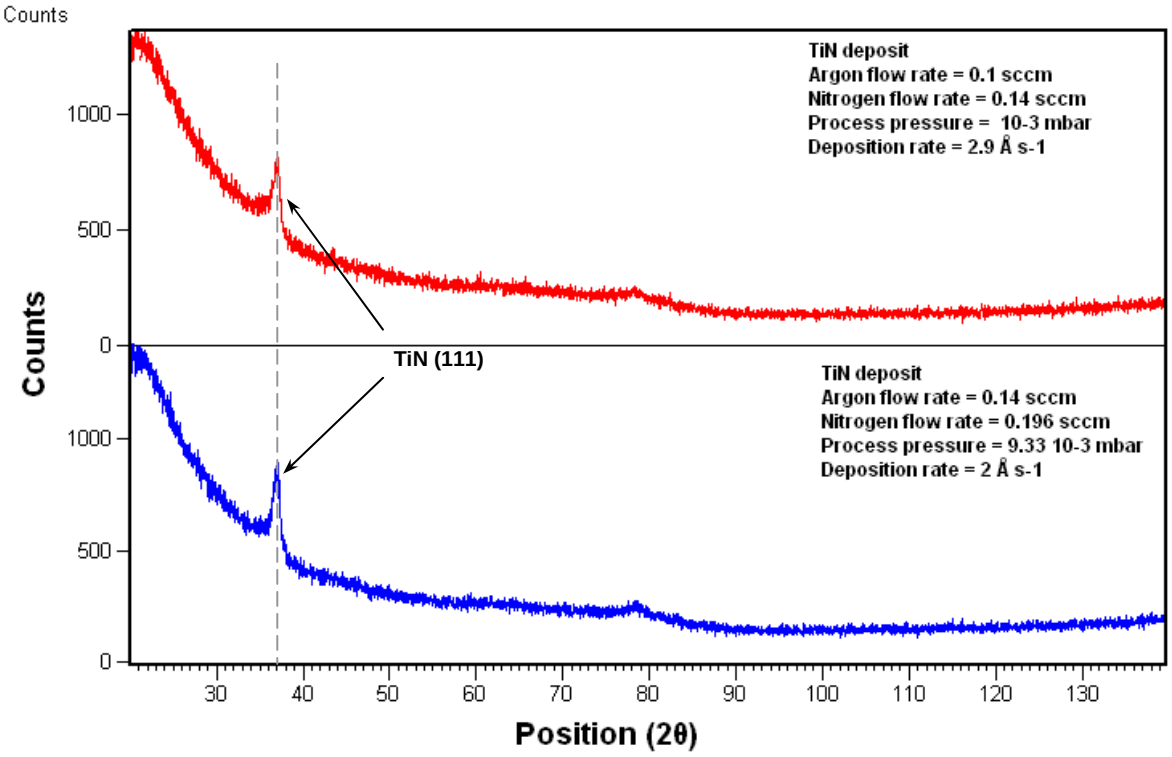

Figure III-3: *XRD plots of two TiN deposits made at different flow rate of argon and nitrogen with respect of stoichiometric ratio.*

The both curves show an intense peak at 2θ = 36.7°, relative to the plan orientation (111) of TiN indicating that the stoichiometries of both deposit is respected. We note that the preferential orientation (220) observed in Figure III-1 has disappeared.

Observing results in table III-2, we note that the deposition rate decrease when pressure process increase. This dependence is quit linear (Figure III-4), which means that even when process pressure change for a given argon and nitrogen flow rate setting (due to base pressure change or a better getter effect of the vacuum chamber's walls), we can estimate the deposition rate and so the time required for a given thickness obtaining.

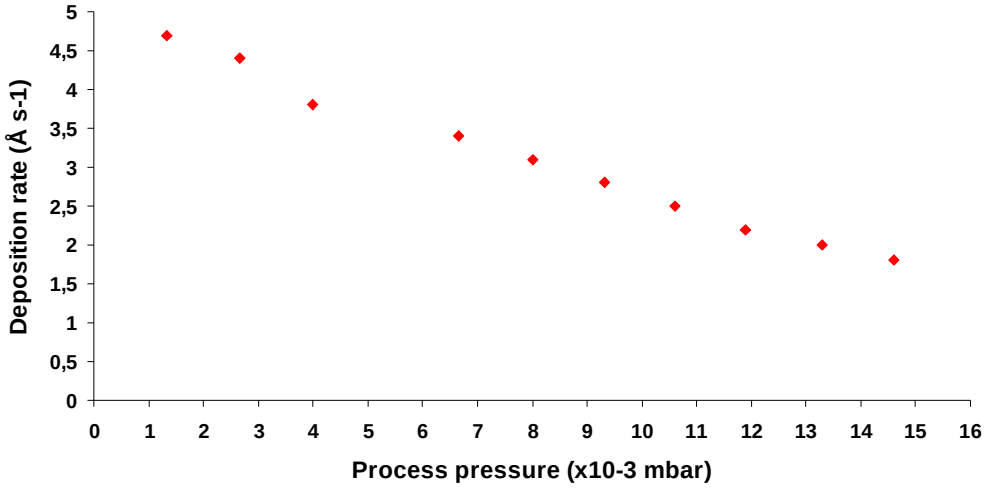

Figure III-4: *Deposition rate dependency with process pressure.*

Results in table III-3 show that by varying the flow rate of argon and nitrogen, we have covered a wide range of operating sputtering pressure, until the limiting borders of process functioning. The middle of this range corresponds to a deposition rate of 3 Å s^{-1}. This value is suitable for the further film deposition, high enough for a quick coating and working in a good pressure condition. Deposition time, t_D given in second, will be calculated according to the following relation:

$$t_D = \frac{10 * e}{V_D} \quad (III\text{-}4)$$

where e is the film thickness (nm), and V_D the rate deposition (Å s^{-1}).

IV- Thickness control of stoichiometric deposit

As we have explain previously (*Cf. §I- III- Multipactor suppressor thin film*), in addition to stoichiometry, film thickness is an important parameter to control so that the multipactor suppressor layer doesn't constrain the efficient functioning of ceramic windows.

As we have seen in sputtering system description, a quartz microbalance is integrated to the bench allowing an in-situ monitoring of deposition rate and film thickness. However, the quartz crystal placed at the internal of vacuum chamber, is oriented in such way that it receive sputtered atoms from both targets (figure III-5).

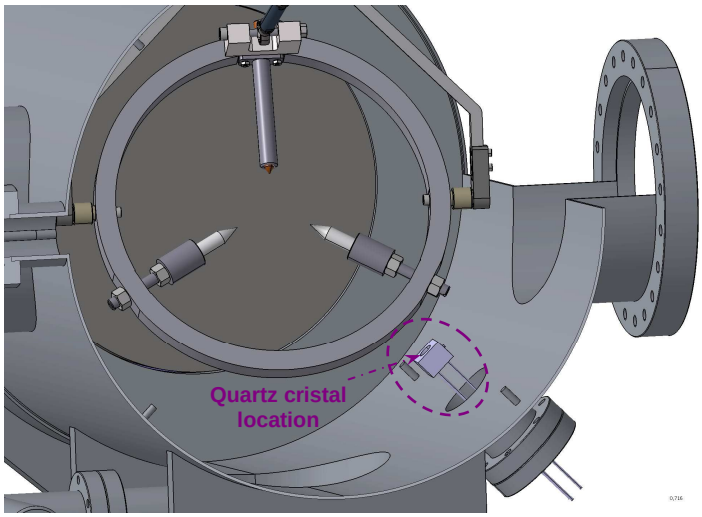

Figure III-5: *Section view of vacuum chamber with the localisation of quartz crystal holder.*

Certainly, this configuration permits a good monitoring of the deposition in internal and external faces of cylindrical samples, but may be not the samples receiving deposit just from one target as it is the case of quartz samples (figure III-1). That's why, a correlation must be found between the film thickness estimated by microbalance and the real value obtained on the substrate.

Several thin deposits are made for different deposition rate and/or different time deposition, then analysed by X-ray reflectivity to measure their thickness and thus correlate them to the value given by microbalance. Figure III-6 shows the reflectivity curves of those samples.

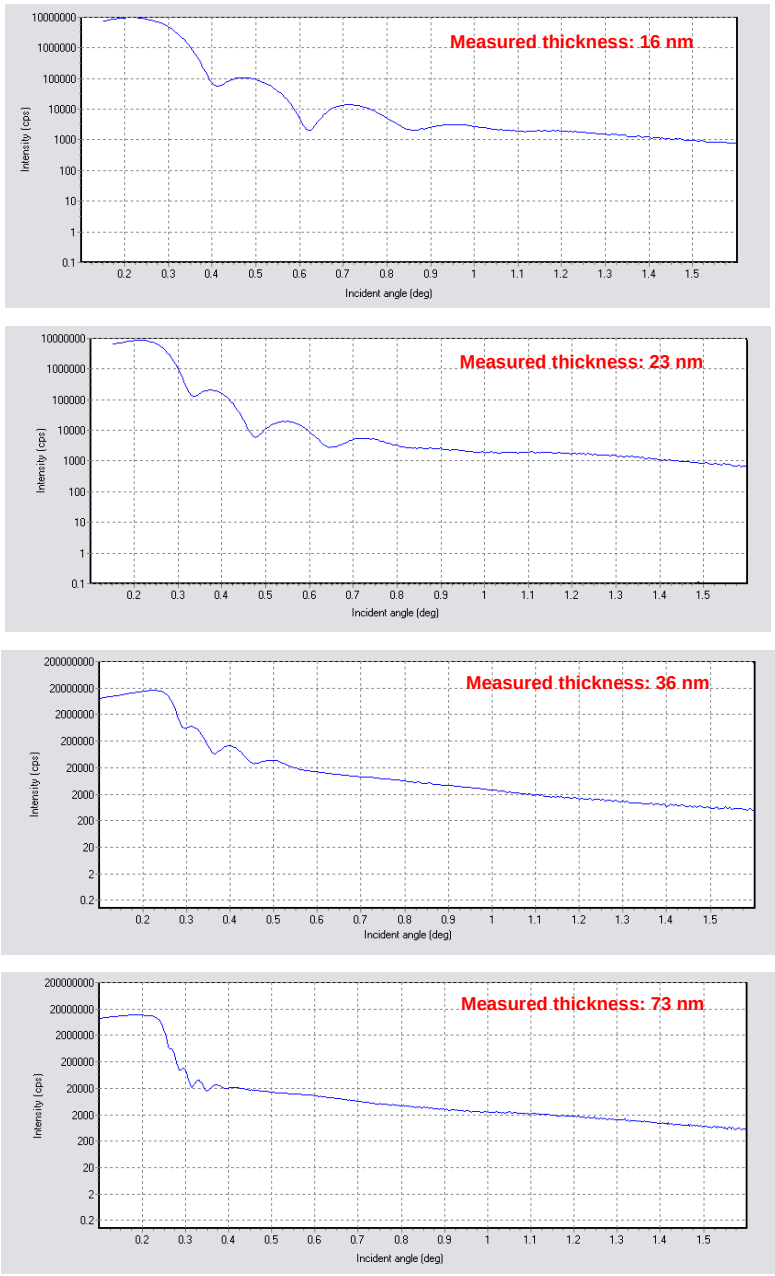

Figure III-6: *Reflectivity curves for TiN deposits at different thickness.*

Before presenting the results of these experiences, let's describe briefly the shape of reflectivity curve to better understand the information it provide.

After a first flat top at little angle, relative to total reflection of the deposit, we observe a succession of interference fringes having the same width that are gradually attenuated till disappear because of the interface deposit-substrate roughness. The width of the oscillation gives the thickness of the deposit and the calculation is based on geometrical optic rules.

The fringe width is inversely proportional to the film thickness: the more the layer is thin the largest is the fringe width and inversely.

A simulation soft allow as the determination of electronic density, substrate and film roughness, and layer thickness. If the first two film characteristics still somewhat approximated, the third one is very precise. In the following table we present the results of the subsequent analysis making a comparison with the thickness estimated by the microbalance.

Table III-4: *Reflectivity simulated curve results and comparison between expected thickness (µ-balance) and measured one*

Expected thickness (nm)	Mesured thickness (nm)	Density (g cm-3)	Roughness (nm)
16.2	**16.2**	**4.4**	**1.9**
23.4	**23**	**3.48**	**2**
36.0	**37**	**3.4**	**3.9**
71.1	**72**	**3.09**	**7**

A very good agreement is found between real thicknesses measured by X-Ray reflectivity and estimated one from microbalance. In fact, the difference between the two values doesn't exceed 3% in all exploitable range. Thus, the fact that quartz crystal emplacement allow the coating from both target is compensated by the position of our samples in front of the target. This result is very important since for a cylindrical window placed in the middle of the chamber without moving, we can have the same deposit thickness in internal and external side of the cylinder receiving deposit from both target, and on the bottom and top grooves exposed to only one target. The movement of the sample holder (*§$_{II}$- II-4- Sample holder*) will assure the difference of thickness between those two part as it is required (*§$_{II}$- I-1- General requirement*).

Concerning the density values, we note than the measured value are lower than the density of bulk TiN (5.79 g cm-3). This was predictable regarding the thickness of the layer we deposit and the difference of properties between bulk and thin layers.

V- Influence of substrate-target distance on sputtered films

The study of substrate to target distance variation is an important field to investigate when working on reactive sputtering. Schiller et al. [38] published an experimental investigation of this effect in a paper covering many important aspects of controlling the deposition process between the metallic and reactive modes of the target. They conclude that optimisation of substrate to target distance can reduce target poisoning effect and allows reaching the stoichiometric composition with a low flow rate of reactive gas.

In our case, the approach is different since the sputtering will occurs with ceramic window placed in the middle of vacuum chamber at an equal fixed distance of both targets. The aim of this experiment is to shows if the sputtering process is uniform or not along the axis of vacuum chamber. Both stoichiometry and thickness will be studied.

For this purpose, a special sample holder is designed to fix 10x10 mm class samples at different distance from the targets (figure III-7).

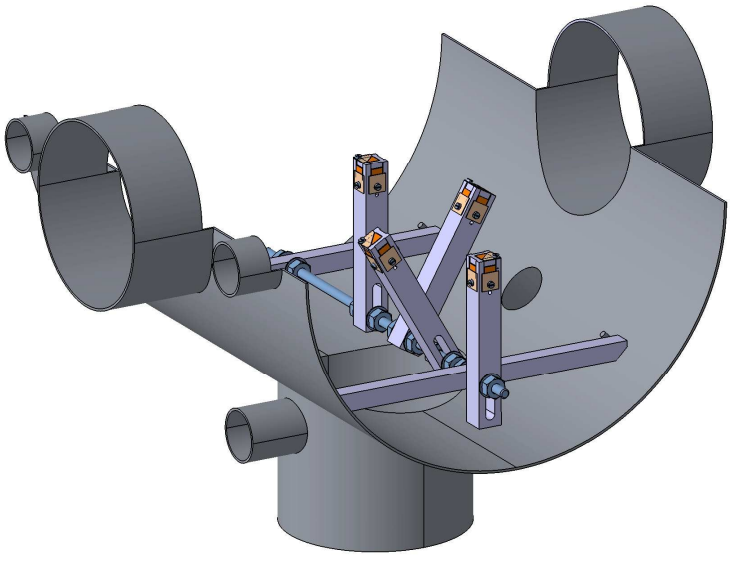

Figure III-7: *Section view of vacuum chamber with a special sample holder allowing the study of target-substrate distance variation influence in sputtering process*

V-1- Influence on deposit stoichiometry

Reactive sputtering of titanium nitride is done in the following conditions:

- Argon flow rate = 0.1 sccm;
- Nitrogen flow rate = 0.14 sccm;
- Bias current = 3 A;
- Base pressure = 2.4 10^{-6} mbar;
- Process pressure = 5.33 10^{-3} mbar;
- Deposition rate = 3 Å s^{-1};
- Deposition time = 30 min;
- 6 samples at respectively d_1 = 6.5 cm, d_2 = 11.5 cm, d_3 = 16.5 cm, d_4 = 22 cm, d_5 = 25.5 cm, d_6 = 35.5 cm.

Obtained films are analysed by X-Ray diffraction, then the lattice parameter and the N/Ti ratio is calculated. Results are summarized in the following table:

Table III-5: *influence of target to sample distance on lattice parameter and N/Ti ratio*

	Distance target-sample (cm)	d (111) (Å)	a (Å)	x (TiNx)
Sample 1	6.5	2.4238	4.1981	0.12
Sample 2	11.5	2.4447	4.2343	0.89
Sample 3	16.5	2.4472	4.2387	0.99
Sample 4	22	2.4257	4.2015	0.19
Sample 5	25.5	2.4335	4.2149	0.48
Sample 6	35.5	2.4733	4.2839	1.95

Results show clearly the influence of the distance between the target and a sample on the stoichiometry of the deposit it receives. Before discussing the results, we should precise that x, the N/Ti ratio was calculated according to the equation (*III-3*) valid for $0.6 < x < 1$. The values over that range will not be precise at all and thus will not be taken into account. We will just put the x value as an indication.

When the target to sample distance is small, the flux density of sputtered Ti is so high that the nitrogen flux rate is not sufficient to form stoichiometric deposit, and thus the deposit is under-stoichiometric. As the distance increases, a good agreement between Ti flux density and N_2 flux rate allows a good reactive reaction and x become close to 1.

When the distance become so large (sample 6), the Ti flux density become lower and the deposit become gas rich.

The values obtained for samples 4 and 5 are completely unexpected, one explanation can be the fact that their emplacements in the vacuum chamber are so close from pumping conduct.

V-2- Influence on deposit thickness

To perform this experience, reactive sputtering of titanium nitride was done in the same conditions described above. Only the deposition time changes to 68 s in order to have thin deposit films. Reflectivity analyses are done and the results are shown in the following table:

Table III-5: *influence of target to sample distance on deposit thickness*

	Distance target-sample (cm)	Thickness(Å)	Density (g cm-3)	Roughness (Å)
Sample 1	6.5	50	4.25	4
Sample 2	11.5	36	4.1	3.5
Sample 3	16.5	26	3.2	3.9
Sample 4	22	21.2	4.1	2.8
Sample 5	25.5	16	3.8	2.9

Results show clearly an influence of target to sample distance on deposited film thickness. Regardless of film stoichiometry, the more the sample is close to the target, the thick it will be. To better visualise this dependency, we plot the results in Figure III-8:

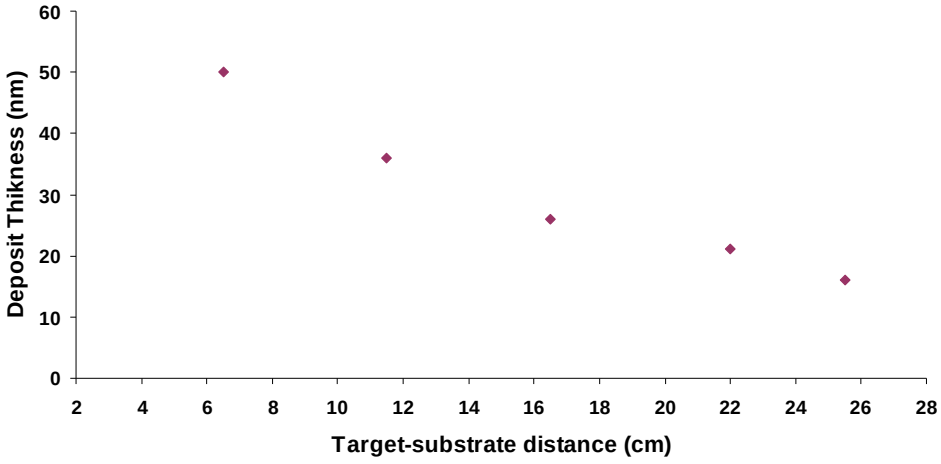

Figure III-8: *Film thickness dependence on target to substrate distance*

As we can see in figure III-8, target to substrate distance influence on thickness deposit is important at low value. Once the distance become larger, this influence is attenuated.

This result may seem constraining for deposition on cylindrical ceramic windows as deposit will not be uniform along its axis, but one should precise that these thicknesses are obtained from only one target while a window will receive sputtered atoms from both. Thus, a little surface of the cylinder localised at d_1 from the first target and d_2 from the second will receive a thickness equal to $TH = th_1 + th_2$ (th_1 from first target and th_2 from the second). The thickness TH should be equal to the one received by a little surface at the middle of the cylinder from the two target.

Conclusions

Conclusions

In the framework of a joint research activity, an innovative design of a sputtering coating bench has been realised by LNL-Legnaro and LAL-Orsay. The goal was to be able to coat different geometry of Alumina windows (planar and cylindrical) with nanometric and stoechiometric TiN films.

A first step of reactive gas flow rate optimisation was done to reach stoichiometric deposit conditions. XRD analyses were performed on 400 to 500 nm layers and lattice parameters of the deposits were determined to deduce N/Ti ratio. Stoichiometric condition was reached for an N_2 flow rate of 0.14 sccm with a fixed Ar flow rate of 0.1 sccm and an imposed current bias of 3A.

By fixing the ratio f_{Ar}/f_{N2} as for stoichiometric condition, the influence of process pressure on deposition rate was studied. The later was seen to decreases when process pressure increases, and the dependence was quit linear. This tendency allows us to predict deposition rate by a lecture of the pressure. This can be useful in case on deposition of very thin films.

As the thickness is an important parameter to monitor, and because of the orientation difference in the vacuum chamber between microbalance quartz crystal and the sample to be coated, X-Ray reflectivity analyses were performed to measure the deposit thickness and find a correlation between microbalance results and the real thicknesses. Results show a very good agreement between both measurements, which mean that quartz crystal emplacement allowing the coating from both target is compensated by the position of our samples in front of the target.

An important influence of the target to substrate distance was found on both thickness and stoichiometry of the film. This is due to the difference of sputtered titanium emission flux and its consequence on reactive reaction establishment.

References

[1] H. Jenhani, «Conditionnement des coupleurs de puissance HF pour cavités supraconductrices an modes pulsé», Journées jeunes chercheurs 2004, île Berder, Bretagne, France.

[2] I. E. Campisi, «State of the Art Power coupler for superconducting RF Cavities», EPAC 2002, Paris, France.

[3] «The european X-Ray Free-Electron Laser technical design report», DESY 2006-097, Germany, July 2006.

[4] T. Garvey, «The design and performance of CW and pulsed power coupler- a review», SRF 2005, USA, Physica C411 (2006) 209-215.

[5] H. Jenhani, «Coupleurs de puissance HF pour cavités supraconductrices an modes pulsé », Thesis 2006, Laboratoire de l'Accélérateur Linéaire (LAL), Orsay, France.

[6] F. Hohn et al. «The transition of a multipactor to a low-pressure gas discharge», Phys. Plasmas, 4-4 (1997) 940-944.

[7] T. P. Graves et al. «Effect of multipactor discharge on alcator c-mod ion cyclotron range of frequency heating» J. Vac. Sci. Tech. A, 24-3, (2006) 512-516.

[8] J. D. Cobine «Gaseous Conductors». Dover Publications, Inc. New York, 1958.

[9] Suharyanto et al. « Secondary electron emission of TiN-coated alumina ceramics» vacuum 81-6 (2007), 799-802.

[10] S. Michizono et al. «Secondary electron emission of sapphire and anti-multipactor coatings at high temperature» Applied Surface Science 235 (2004) 227-230.

[11] T. P. Graves, «Experimental investigation of electron multipactor discharges at very high frequency», Thesis 2006, Massachusetts Institue of Technology (MIT), Cambridge, USA.

[12] E. Somersalo et al. «Electron Multipacting in RF structures», TESLA Report, (1994), 14-94.

[13] F. L. Krawczyk, «Status of Multipacting simulation capabilities for SCRF applications», SRF 2001, Japan.

[14] W. D. Sproul, «High-rate reactive DC magnetron sputtering of oxide and nitride superlattice coatings», Vacuum 51-4, (1998), 641-646.

[15] J. Musil et al. IPAT 87 Proceeds of the 6th International Conference on Ion and Plasma Assisted Techniques, Brighton UK, (1987), 184–189

[16] A. Rizk, «Glow discharge characteristics when magnetron sputtering copper in different plasma atmospheres operated at low input power», Vacuum 38-2, (1988), 93-95.
[17] J. L. Vossen et al. J. Vac. Sci. Technol. A 9-3, (1991) 600-603.

[18] S. Kadlek et al. «Hysteresis effect in reactive sputtering: a problem of system stability» J. Phys. D: Appl. Phys. 19, (1986), L187- L190.

[19] I. Safi «Recent aspects concerning DC reactive magnetron sputtering of thin films: a review», Surface and Coating Technology 127, (2000), 203-219.

[20] S. Maniv et al. « Discharge characteristics for magnetron sputtering of Al in Ar and Ar/O2 mixtures», J. Vac. Sci. Techno. 17-3, (1980), 743-751.

[21] S. Maniv et al. «Oxidation of an aluminium magnetron sputtering target in Ar/O2 mixtures» J. Appl. Phys. 51-1, (1980), 718-725.

[22] A. J. Aronson et al. «Preparation of titanium nitride by a pulsed d.c. magnetron reactive deposition techniques using the moving mode of deposition» Thin solid films, 72-3, (1980), 535-540.

[23] A.Ruiz et al. «UHV reactive evaporation grouth of titanium nitride thin film, looking for multipactor effect suppression in space applications», Vacuum 81, (2007), 1497-1497.

[24] A. R. Nyaiesh et al. «Properties of thin antimultipactor TiN and Cr_2O_3 coating for klystron windows», J. Vac. Sci. Technol. A, 4-5 (1986) 2356-2363.

[25] G.G. Fuentes et al. «Spectroscopic investigations of Cr,CrN and TiCr anti-multipactor coatings grown by cathodic-arc reactive evaporation», Applied Surface Science 253, (2007), 7627-7631.

[26] J. Lorkiewicz et al. «Anti-multipactor TiN coating of RF power coupler components for TESLA at DESY», Tesla Report 2004-02, DESY, Hambourg, Germany.

[27] A. R. Nyaiesh et al. «Properties of thin anti-multipactor coating for klystron windows», SLAC-Pub-3760 (1985).

[28] J. G. Power et al. «Experimental study of multipactor suppression in dielectric-loaded accelerating structure», Advanced Accelerator Concepts Eleventh Workshop, American Institute of Physics (2004).

[29] N. Mustapha et al. «Optical TiN films by filtered arc evaporation», Surf. Coat. Technol. 92, (2007), 29-33.

[30] K. Lal et al. «Electrical resistivity of titanium nitride thin films prepared by ion beam-assisted deposition», Phisica B, 307, (2001), 150-157.

[31] L. Fouilland et al. «Composition and tribological characterization of chemically vapour-deposited TiN layer», Surf. Coat. Technol. 100-101, (1998), 146-148.

[32] V. Cracium et al. « Growth of thin transparent titanium nitride layers by reactive laser ablation», Appl. Surf. Sci. 138-139, (1999), 593-598.

[33] J. H. Huang et al. «Effect of nitrogen flow rate on structure and properties of nanocrystalline TiN films produced by unbalanced magnetron sputtering», Surface & Coating Technology, 191, (2005), 17-24.

[34] Y. L. Jeyachandran et al. «Properties of titanium nitride films prepared by direct current magnetron sputtering», Materials Science and Engineering A, 445-446 (2007), 223-236.

[35] H. H. Huang et al. «Effect of nitrogen flow rate on growth and properties of titanium nitride films obtained by atmospheric pressure chemical vapour deposition», Thin Solid Films, 416, (2002), 54-61.

[36] S. Nagakura et al. «Lattice parameter of the non stoichiometric compound TiN_x», J. Appl. Cryst. 8 (1975), 65-66.

[37] V. Valvoda et al. «Dependence of microstructure of TiN coatings on their thickness», Thin Solid Films, 158-2 (1988), 225-232.

[38] S. Schiller et al. Thin Solid Films, 111, (1984), 259-268.